Published in final edited form as:

Structure. 2019 June 04; 27(6): 1013–1021.e3. doi:10.1016/j.str.2019.03.003.

Ion and pH Sensitivity of a TMBIM Ca^{2+} Channel

Gongrui Guo[1,2,#], **Min Xu**[3,#], **Yanqi Chang**[4,#], **Tomas Luyten**[5], **Bruno Seitaj**[5], **Wu Liu**[1,2], **Ping Zhu**[1], **Geert Bultynck**[5], **Lei Shi**[3,*], **Matthias Quick**[6,7,*], and **Qun Liu**[1,2,8,*]

[1]Biology Department, Brookhaven National Laboratory, Upton, NY, 11973 USA.

[2]NSLS-II, Brookhaven National Laboratory, Upton, NY, 11973 USA.

[3]Computational Chemistry and Molecular Biophysics Unit, National Institute on Drug Abuse - Intramural Research Program, National Institutes of Health, Baltimore, MA 21224, USA.

[4]New York Consortium on Membrane Protein Structure, New York Structural Biology Center, New York, NY 10027, USA.

[5]Laboratory Molecular and Cellular Signaling, Department Cellular and Molecular Medicine, Campus Gasthuisberg O/N-I bus 802, Herestraat 49 BE-3000 Leuven, Belgium.

[6]Department of Psychiatry, Columbia University College of Physicians and Surgeons, New York, NY 10032, USA.

[7]Division of Molecular Therapeutics, New York State Psychiatric Institute, New York, NY 10032, USA.

[8]Lead Contact

Summary

The anti-apoptotic transmembrane Bax inhibitor motif (TMBIM) containing protein family regulates Ca^{2+} homeostasis, cell death, and diseases including cancers. The recent crystal structures of the TMBIM homolog BsYetJ reveal a conserved Asp171-Asp195 dyad that is proposed in regulating a pH-dependent Ca^{2+} translocation. Here we show that BsYetJ mediates Ca^{2+} fluxes in permeabilized mammalian cells, and its interaction with Ca^{2+} is sensitive to protons and other cations. We report crystal structures of BsYetJ in additional states, revealing the flexibility of the dyad in a closed state and a pore opening mechanism. Functional studies show that the dyad is responsible for both Ca^{2+} affinity and pH dependence. Computational simulations

*Correspondence: lei.shi2@nih.gov (L.S.), mq2102@cumc.columbia.edu (M.Q), or qunliu@bnl.gov (Q.L.).
#These authors contribute equally to the work

Author Contributions

L.S., M. Q., G.B, and Q.L. designed the study and experiments. G.G., M.Y., Y.C., T.L., B.S., W.L., P. Z., M.Q., and Q.L. performed the experiments. All authors contributed to data analyses. Q.L., M.Q., and L.S. wrote the manuscript with help from others.

Supplemental Information

Supplemental information includes one figure. Document S1. Figure S1

Declaration of Interests

The authors declare no competing interests.

suggest that protonation of Asp171 weakens its interaction with Arg60, leading to an open state. Our integrated analysis provides insights into the regulation of the BsYetJ Ca^{2+} channel that may inform understanding of human TMBIM proteins for their roles in cell death and diseases.

Graphical Abstract

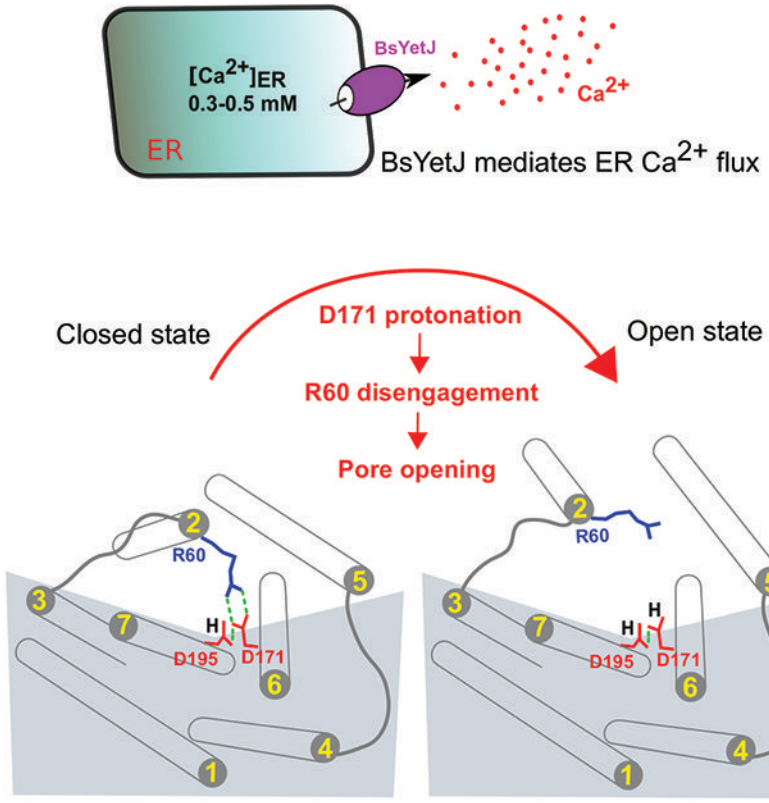

eTOC:

Guo et al. present structural, functional, and computational analyses on a bacterial TMBIM Ca^{2+} channel BsYetJ. They show that BsYetJ mediates Ca^{2+} flux in mammalian cells, and its Ca^{2+} binding is sensitive to protons and other cations. The conserved aspartyl dyad regulates Ca^{2+} binding, pH sensing, and the channel pore opening and closing.

Introduction

Transmembrane Bax Inhibitor Motif (TMBIM) containing proteins are a family of membrane proteins that control Ca^{2+} flux across membranes to maintain Ca^{2+} homeostasis in subcellular Ca^{2+} stores (Ahn et al., 2009; Rojas-Rivera and Hetz, 2015; Gamboa-Tuz et al., 2018). TMBIM proteins are highly conserved and ubiquitously expressed in both pro- and eukaryotic cells, as well as in viruses and archaea (Figure S1) (Henke et al., 2011; Chang et al., 2014). TMBIM proteins have been shown to be associated with the suppression of cell death in response to a broad spectrum of stresses in plants and intrinsic and extrinsic programmed cell death in mammals (Reimers et al., 2008; Hu et al., 2009; Henke et al., 2011; Ishikawa et al., 2011; Lisak et al., 2015). An increasing number of studies suggest that

the suppression of cell death by TMBIM proteins is directly or indirectly linked to their roles in maintaining Ca^{2+} homeostasis (Carrara et al., 2015; Rojas-Rivera and Hetz, 2015; Lisak et al., 2016; Liu, 2017; Luganini et al., 2018).

TMBIM proteins were originally identified from phenotypic screening of anti-apoptotic human genes in yeast overexpressing Bax, a proapoptotic protein killing yeast cells (Xu and Reed, 1998). Although there are no direct interactions between Bax and TMBIM proteins, anti-apoptotic Bcl-2 family members, such as Bcl-2 and Bcl-xL, have been alluded to interact with TMBIM proteins by co-immunoprecipitation (Xu and Reed, 1998; Urresti et al., 2016). The interactions and functional overlapping of TMBIM and Bcl-2 family proteins may provide multi-layered and redundant protections of cellular survival in response to stress signals including Bax overexpression. In humans, there are six members (TMBIM1-6) localized in diverse cellular and subcellular membranes. These proteins are dysregulated in multiple cancers (Grzmil et al., 2006; Lu et al., 2015; Rojas-Rivera and Hetz, 2015; Carrara et al., 2017). TMBIM4 and 6 are upregulated in brain, breast, and prostate cancers; they are downregulated in leukemia and colorectal cancer (Carrara et al., 2017). As a contrast, TMBIM3 is upregulated in colorectal and gastric cancer, while TMBIM1 is downregulated in leukemia, breast, and sarcoma cancers (Rojas-Rivera and Hetz, 2015). In addition to their abnormal expression in cancers, TMBIM proteins have been described with additional cellular functions. TMBIM1 is upregulated in response to mechanical stress (Yoshisue et al., 2002; Shukla et al., 2011). TMBIM2 over-expression protects against transient brain ischemia (Reich et al., 2011) and increases axon growth (Merianda et al., 2013). TMBIM4 and TMBIM6 regulate cell adhesion and migration through Ca^{2+}-dependent mechanisms (Lee et al., 2010; Saraiva et al., 2013; Carrara et al., 2015). Located in the mitochondrial inner membrane, TMBIM5 regulates mitochondrial fragmentation and cytochrome c release (Oka et al., 2008). TMBIM6 protects against acute brain injury (Krajewska et al., 2011), promotes autophagy (Sano et al., 2012) and enables immune cell survival and function (Lisak et al., 2016). TMBIM3 and TMBIM6 may interplay with each other and synergistically mediate unfolded protein response and autophagy (Rojas-Rivera et al., 2012).

Most TMBIM-mediated cellular functions relate to their core roles in Ca^{2+} flux and Ca^{2+} homeostasis (Lisak et al., 2015; Carrara et al., 2017). TMBIM6 is able to mediate the passive leak of Ca^{2+} from the ER, hence its classification as a Ca^{2+} leak channel (Kiviluoto et al., 2013; Bultynck et al., 2014). This property of TMBIM6 lowers steady-state ER Ca^{2+} levels in TMBIM6-overexpressing cells (Chae et al., 2004; Xu et al., 2008). Similarly TMBIM4 lowers the content of ER and Golgi Ca^{2+} stores and enhances store-operated Ca^{2+} entry (de Mattia et al., 2009; Saraiva et al., 2013; Carrara et al., 2015).

Thus, a common feature of TMBIM proteins in cells is their ability to prevent the overloading of intracellular Ca^{2+} stores. This feature reduces the likelihood for Ca^{2+} overload and excessive Ca^{2+} fluxes into mitochondria to occur, thereby promoting cell survival and rendering cells more resistant to cell death stimuli (Pinton et al., 2008). In TMBIM4 and 6, several critical aspartate residues were identified to establish an assumed Ca^{2+}-permeable channel pore near its C-terminus (Bultynck et al., 2012; Carrara et al., 2015). Originally, it was proposed that TMBIM6's basal channel function was promoted by low pH, suggesting it would act as a H^+/Ca^{2+} exchanger (Kim et al., 2008). However,

follow-up work showed that low pH is actually abrogating Ca^{2+} flux through the Ca^{2+}-permeable pore (Kiviluoto et al., 2013). However, due to challenges in obtaining mammalian TMBIM structural information, the molecular determinants leading to pore opening and closing and thus the underlying Ca^{2+} flux properties of TMBIM proteins remained unclear (Bultynck et al., 2012; Bultynck et al., 2014; Carrara et al., 2015). This has recently changed with the determination of the structures of a bacterial homolog of TMBIM proteins from *Bacillus subtilis,* BsYetJ (Chang et al., 2014). These structures reveal a unique fold of 7 transmembrane helices (TM) with its second transmembrane helix (TM2) capable of opening and closing laterally within the membrane bilayer. An aspartyl dyad that is conserved among all TMBIM members (Asp171-Asp195 in BsYetJ) (Figure S1) was proposed to be a pH sensor regulating the pore dynamics and Ca^{2+} translocation (Chang et al., 2014).

Here we present crystal structures of BsYetJ wild-type and variants with mutations of Asp171 or Asp195. Together with functional and computational studies we show the ion- and pH-dependent modulation of BsYetJ activity and provides insights into the core mechanism of the conserved Asp171- Asp195 dyad being the structural determinant that leads to the opening of this Ca^{2+} leak channel.

Results

BsYetJ can mediate Ca^{2+} efflux from eukaryotic intracellular Ca^{2+} stores

We have previously solved structures of a bacterial homolog BsYetJ and demonstrated its Ca^{2+} flux activity in *E. coli* overexpressing BsYetJ and proteoliposomes with reconstituted BsYetJ (Chang et al., 2014). Sequence alignment studies revealed that the proposed pH-sensing aspartyl-dyad (Asp171- Asp195 in BsYetJ) is a conserved feature found in TMBIM proteins across all kingdoms (Chang et al., 2014). To study the functional conservation of BsYetJ in mediating Ca^{2+} flux in eukaryotic cells, we assessed whether purified BsYetJ protein could promote $^{45}Ca^{2+}$ efflux from the ER of human cells, similarly to what was previously observed for synthetic peptides derived from the TMBIM6 C terminus (Bultynck et al., 2012). We performed unidirectional $^{45}Ca^{2+}$ flux assays in permeabilized HeLa cells. After saponin-mediated permeabilization of the HeLa cells and loading the ER Ca^{2+} stores to steady state with $^{45}Ca^{2+}$, we washed the cells with thapsigargin, an inhibitor of the sarco/endoplasmic reticulum Ca^{2+}-ATPase (SERCA), and monitored the unidirectional $^{45}Ca^{2+}$ efflux from the ER Ca^{2+} stores. The resulting data are plotted as Ca^{2+} release and $^{45}Ca^{2+}$ content as function of time (Figures 1A, B). Notably, addition of 2.5 μM BsYetJ provoked a major increase in the $^{45}Ca^{2+}$ release (Figure 1A), a phenomenon that was not observed in the control condition, i.e. the addition of buffer without BsYetJ. This could also be observed as a drop in the $^{45}Ca^{2+}$ content upon addition of the BsYetJ protein (Figure 1B). There was a delay in the BsYetJ-associated response, likely related to the time needed for BsYetJ protein to incorporate into the ER membranes. Therefore, bacterial BsYetJ, when added to permeabilized human HeLa cells, may reconstitute to the membranes of intracellular Ca^{2+} stores, thereby functioning as Ca^{2+}-permeable channel-like proteins that mediate Ca^{2+} flux across membranes.

Inhibition of Ca^{2+} binding by ions.

To further characterize the substrate specificity profile of BsYetJ, we used scintillation proximity assay (SPA)-based binding of $^{45}Ca^{2+}$ (Quick and Javitch, 2007; Zehnpfennig et al., 2015) in the presence or absence of several physiologically relevant cations. Whereas binding measurements performed in assay buffer containing high concentrations of Na^+ (100 mM) revealed virtually no Ca^{2+} binding, in absence of Na^+, however, robust binding of $^{45}Ca^{2+}$ was observed (Figure 1C). Ca^{2+} binding was pH dependent in bell-shaped fashion, with higher activity at pH 7.5 and lower activity at pH 6 and 8. This result is consistent with our Ca^{2+} flux assays in proteoliposomes reported previously (Chang et al., 2014). Fitting the pH dependence of $^{45}Ca^{2+}$ binding to a Gaussian model revealed a peak at pH 7.5 (Figure 1C). It is noteworthy to mention that even though the activity at 7.5 was higher than that observed at pH 6.0, substantial activity was still detectable at the latter pH, suggesting that BsYetJ activity is regulated by pH. Measuring the isotopic dilution of $^{45}Ca^{2+}$ bound to BsYetJ with increasing concentrations of non-labeled Ca^{2+} at pH 7.5 revealed a reduction of the bound $^{45}Ca^{2+}$ by 50 % (EC_{50}) at a concentration of 65.4 μM of $CaCl_2$ (Figure 1D). Since Ca^{2+} has an ionic radius of 0.99 Å which is very close to Na^+ with an ionic radius of 0.98 A, we speculated that the concentration of Na^+ that reduces $^{45}Ca^{2+}$ binding by 50% (IC_{50}) would be comparable to the apparent affinity of Ca^{2+}. However, Na^+, K^+ and Li^+ inhibited $^{45}Ca^{2+}$ binding with IC_{50} of 18.5±5.7 mM, 14.0 ± 3.9 mM, and 16.1 ± 6.5 mM, respectively. The inhibitory effect of the monovalent ions Na^+ and K^+ at physiological concentrations suggests a regulatory mechanism by these ions on the Ca^{2+} leak activity of BsYetJ.

To further expand the ion regulation profile of BsYetJ, we measured $^{45}Ca^{2+}$ binding in the presence of 5 mM each of Mg^{2+}, Mn^{2+}, Gd^{3+}, Yb^{3+}, and Lu^{3+} by using the SPA. We found that Mg^{2+} and Mn^{2+} had no apparent inhibition of Ca^{2+} binding (Figure 1E), while Yb^{3+} and Lu^{3+}, and most notably Gd^{3+}, inhibited Ca^{2+} binding. Among these lanthanides, Gd^{3+} has a much stronger inhibitory potency than Yb^{3+} and Lu^{3+}. Measuring the concentration dependence of Gd^{3+} on $^{45}Ca^{2+}$ binding revealed an IC_{50} of 24.2 ± 2.8 μM. It is possible that in addition to competing with Ca^{2+} for binding to the proposed Ca^{2+} binding site, Gd^{3+} might bind specifically to a remote site which may induce conformational changes unfavorable of Ca^{2+} binding.

Alternative pH-sensor structure determined in lipidic cubic phase

To understand the delicate structure of the pH-sensing unit in a native-like lipidic environment, we crystallized wild-type BsYetJ in lipidic cubic phase (LCP) and determined its structure at 2.5 Å resolution by molecular replacement. Figure 2A shows the superposition of the BsYetJ structure crystalized in LCP (^{LCP}BsYetJ) on its structure crystallized in the detergent pentaethylene glycol monodecyl ether (C10E5) (^{C10E5}BsYetJ). Both structures are in a closed conformation with an RMSD of 0.64 Å. The relatively large rearrangements are the two loops connecting to TM2, consistent with the required flexibility of TM2 capable of lateral movement in the conformational transition between open and closed states (Chang et al., 2014). In addition, some side chains adopt different rotamer conformations (Figure 2A), likely due to either interactions with lipids or detergents, or lattice packing. The structure in closed conformation is featured by the proximity of residues Arg60, Asp171, and Asp195 (Figure 2B). To see structural difference of the proposed pH-

sensing dyad (Asp171-Asp195) in ^{LCP}BsYetJ and ^{C10E5}BsYetJ, we superimposed the two structures based on their Cα atoms on TM7 (Figure 2C). In the ^{LCP}BsYetJ structure, the distance between the Asp171 and Asp195 carboxylates is 2.9 Å, indicating the coupling of the two carboxylates and the protonation of Asp195 as a proton donor in hydrogen bonding. This is consistent with the corresponding H-bond in the ^{C10E5}BsYetJ structure. However, surprisingly, the side chains of Asp171 and Asp195 in ^{LCP}BsYetJ deviate from their respective positions in ^{C10E5}BsYetJ. Consequently, the two H-bond distances between Arg60 and Asp171 in ^{LCP}BsYetJ are longer than these in ^{C10E5}BsYetJ. Considering that the ^{LCP}BsYetJ structure is in a native-like environment, these relative movements show structural flexibility of these three residues even in the closed state.

To induce potentially more drastic changes, we attempted soaking ^{LCP}BsYetJ crystals at pH 6 and 7. However, soaked ^{LCP}BsYetJ crystals did not diffract X-rays or even disappeared. This might suggest that the crystallographic lattice ($P2_1$) is not compatible with associated conformational changes. Nevertheless, the alternative conformations of Arg60, Asp171, and Asp195 seeing in ^{LCP}BsYetJ and ^{C10E5}BsYetJ structures show a possible pH-dependent structural transition that leads to pore opening. We can imagine that decreasing pH may increase the protonation probability of Asp171, rendering a structure to be primed for Ca^{2+} flux.

Structure and activities of two pH sensor mutants

To further characterize the channel structurally and biochemically, we made D171E and D195E variant constructs by adding a CH_2 group to the side chains of the dyad residues Asp171 and Asp195. Note these mutations retain the overall charge. In spite of crystallization of both mutants in LCP and detergent, we found that crystals that diffracted to adequate resolutions only from detergent preparations. The two mutant structures are in their open conformations even though they were crystallized at a neutral pH 7.5 (^{D171E}BsYetJ) and 7.0 (^{D195E}BsYetJ) (Figures 3A, B). Both mutants were crystallized in space group C2. The solved structures indicate four molecules in asymmetric unit. In each mutant structure, the four molecules have a Cα RMSD of 0.30-0.71 Å for ^{D171E}BsYetJ and 0.230.61 Å for ^{D195E}BsYetJ. Superimposition of the four molecules indicates most conformational changes involve the movement of TM5 (Figure 3B). In both structures, Arg60 is away from forming a salt bridge with Asp171 (^{D195E}BsYetJ) or Glu171 (^{D171E}BsYetJ). The distances between the carboxylates at positions 171 and 195 range between 2.9 and 4.6 Å, suggesting a rather unstable coupling between the two carboxylate groups, and thus incapable of locking TM2 in a closed conformation through Arg60 engagement. Upon TM2 opening, TM5 may also undergo conformational changes, more dramatically at the C-terminal side with as much as 9° twist between two TM5 helices in ^{D171E}BsYetJ (Figure 3B, left panel). Similar TM5 twists were also seen in ^{D195E}BsYetJ but to a less extent (Figure 3B, right panel).

To test whether the mutations to the pH-sensing dyad affect the interaction of the proteins with Ca^{2+}, we measured $^{45}Ca^{2+}$ binding at different pHs for BsYetJ wild-type as well as the two mutants by SPA (Figure 3C). In contrast to the bell-shaped curve observed for the wild-type, the two mutants displayed reduced Ca^{2+} binding and significantly different pH dependence. Interestingly, the highest activity was measured at the lowest pH tested (pH

6.0), and Ca^{2+} binding was progressively reduced with increasing pH. Performing isotopic dilution of 10 μM $^{45}Ca^{2+}$ binding by BsYetJ wild-type, ^{D171E}BsYetJ, and ^{D195E}BsYetJ at pH 6.5 revealed that the EC_{50} of Ca^{2+} binding by BsYetJ (64.2 ± 1.3 μM) is virtually indistinguishable from that determined at pH 7.5 (Figure 1D). On the other hand, the EC_{50} for ^{D171E}BsYetJ and ^{D195E}BsYetJ determined at pH 6.5 were determined as 1.2 ± 0.1 mM and 1.7 ± 0.3 mM, respectively (Figure 3D). Therefore, both mutants have much weaker Ca^{2+} affinity relative to the wild-type, suggesting that Asp171 and Asp195 play a critical role in BsYetJ function, either by directly interacting with protons and/or Ca^{2+} or by structurally impacting the recognition of these two ions indirectly. Thus, we propose that the change of an aspartate to glutamate on the pH-sensing dyad may have disrupted the sensing mechanism, resulting in constantly open channels with reduced Ca^{2+} affinities.

Protonation state of Asp171 is critical for pore closing and opening

To understand the dynamics and underlying regulation mechanism in response to pH sensing and protonation, we performed extensive and comparative molecular dynamics (MD) simulations. Starting from the closed-state structure, we compared four simulation conditions, with the Asp171 or Glu171 in either deprotonated or protonated state. In the control simulations of the Asp171-deprotonated condition, the Asp171 and protonated Asp195 form a stable dyad; and Asp171 persistently forms a strong salt bridge with Arg60 (Figure 4A). In the Asp171-protonated condition, the protonation of Asp171 not only disrupted the Arg60-Asp171 salt bridge, the conformation of the Asp171-Asp195 dyad is different from the Asp171-deprotonated condition as well (Figure 4B). In the Glu171-deprotonated state, while we observed that the Arg60 formed the salt bridge with Glu171, the additional CH_2 on the side chain of Glu171 resulted in a less optimal dyad with Asp195 and a slight TM2 rearrangement away from TM6 (Figure 4C). In the Glu171-protonated condition, all the interactions among Arg60, Glu171, and Asp195 are lost (Figure 4D). In both Asp171- and Glu171-protonated conditions, the absence of the salt bridge between Arg60 and Asp171/Glu171 caused TM2 to move downward and also away from TM6 (Figures 4B, D). Such movements are obviously in a direction towards the open state. Thus, the results of our MD simulations are consistent with that protonation of 171 facilitates the conformational transition from the closed to the open state.

Discussion

In eukaryotes, cytosolic [Ca^{2+}] is kept very low in the 100 nM range, which enables cells to exploit Ca^{2+} to encode signals with distinct spatiotemporal properties by transiently and locally increasing cytosolic [Ca^{2+}] (Berridge et al., 2003). Ca^{2+} at a low concentration acts as a second messenger and drives a broad variety of cellular processes in response to extracellular stimuli, including exocytosis, contraction, metabolism, transcription, fertilization and proliferation (Berridge et al., 2003). The low cytosolic [Ca^{2+}] is achieved by Ca^{2+}-binding proteins such as parvalbumin and calbindin and by Ca^{2+}-transport systems that pump Ca^{2+} out of organelles such as the ER via SERCA and Golgi via SPCA or that extrude Ca^{2+} to the extracellular environment via plasma membrane Ca^{2+} ATPases (PMCA) or Na^{+}/Ca^{2+} exchangers (Carafoli and Krebs, 2016). Consequently, free Ca^{2+} concentrations in the ER compartments and the extracellular environment are in the ~500 μM and low mM

range, respectively, which are about four orders of magnitude higher than in the cytosol. These stores provide the cells with plenty of Ca^{2+} that is available to use for signaling purposes.

However, overloaded intracellular Ca^{2+} stores can result in excessive Ca^{2+} transfer between the ER and the mitochondria, which can initiate Mitochondria Outer Membrane Permeabilization (MOMP) and subsequent cell death (Mattson and Chan, 2003; Pinton et al., 2008; Leanza et al., 2013). In fact, several oncogenes and tumor suppressors appear to exploit control over the ER Ca^{2+}-filling state as a means to impact cellular fate (Bittremieux et al., 2016). Thus, not surprisingly, the Ca^{2+}-flux properties of TMBIM-family members have been implicated in cell death control (Rojas-Rivera et al., 2012; Kiviluoto et al., 2013; Carrara et al., 2015). Despite their role in these central cellular functions, the molecular events that govern the activity and/or regulation of the TMBIM Ca^{2+} leak channels are not well understood (Sokolov et al., 2007). In the present study, our experimental data show that a bacterial TMBIM homolog BsYetJ can also lead to Ca^{2+} flux from ER Ca^{2+} stores from mammalian cells, suggesting that the Ca^{2+} flux activity of BsYetJ is conserved. Indeed, we previously used yeast polar lipids for BsYetJ-reconstituted Ca^{2+} flux assays, suggesting that BsYetJ is also capable of mediating Ca^{2+} flux in yeast cells (Chang et al., 2014). Interestingly, in humans, there are six known TMBIM proteins localized to different cellular and subcellular membranes (Lisak et al., 2015; Rojas-Rivera and Hetz, 2015; Liu, 2017). Our data present evidence that a bacterial TMBIM homolog can mediate Ca^{2+} fluxes from intracellular compartments of human cells. Moreover, it provides direct evidence that the Ca^{2+}-flux property of TMBIM-related proteins is highly conserved from bacteria to human, indicating that the ability to mediate Ca^{2+} flux is an inherent property of the TMBIM family occurring already very early in evolution (Figure S1). However, it remains to be tested whether BsYetJ could suppress cell death as its mammalian relatives do.

Structurally, BsYetJ and likely the entire TMBIM family are different from canonical Ca^{2+} channels where there is a well-defined oligomeric pore and selectivity filter (Carrara et al., 2017). It has been hypothesized that the C-terminus of human TMBIM6 may form a re-entry loop and harbor a pore for Ca^{2+} flux (Xu and Reed, 1998; Bultynck et al., 2012). In the closed-state ^{LCP}BsYetJ and ^{C10E5}BsYetJ structures, the C-terminus is a transmembrane helix and is wrapped around by six other transmembrane helices. Two species-conserved residues, Asp195 and Asp171 (Figure S1), forms a hydrogen bond and we have hypothesized their roles in pH sensing and Ca^{2+} activity (Bultynck et al., 2014; Chang et al., 2014). In this study, we mutated either residue to a glutamate and showed that such mutation, even though retaining the overall negative charge, was defective to bind Ca^{2+} and lost the pH-dependent profile as the wild-type (Figures 3C, D). Our biochemical and structural data demonstrate that the two aspartate residues are important in defining a Ca^{2+} passage pore, which is permeable for Ca^{2+}. It is noticed that Ca^{2+} affinity can be inhibited by monovalent ions Na^+, K^+, and Li^+. So it is possible that these ions may all affect the binding of Ca^{2+} to the two mutants. In human TMBIM6, mutating Asp213 (equivalent to Asp195 in BsYetJ) to an arginine affected Ca^{2+} flux (Bultynck et al., 2012). Moreover, in contrast to wild-type TMBIM6, its D213R mutant was unable to protect cells against thapsigargin-induced cell death (Kiviluoto et al., 2013). Similarly, in human TMBIM4, mutating Asp219 (equivalent to Asp195 in BsYetJ) to an asparagine also affected the Ca^{2+} flux. Importantly, this D219N

mutant lost its protective role in apoptosis, thus firmly established the connection of Ca^{2+} flux to apoptosis (Carrara et al., 2015). Learning from human relatives, mutants on Asp195 and Asp171 should help to decipher physiological roles of BsYetJ and its homologs in prokaryotes.

In our SPA-based $^{45}Ca^{2+}$ binding assays we found that monovalent ions Na^+, K^+ and Li^+ inhibited Ca^{2+} binding to BsYetJ at physiological concentrations. It is possible that monovalent cations may regulate the basal channel activity of BsYetJ. Whether BsYetJ is also leaky to these monovalent ions is unknown and will be an intriguing question for future research. Interestingly, divalent ions, Mg^{2+} and Mn^{2+} do not show apparent inhibition, suggesting that the channel is more specific to Ca^{2+} perhaps owing to the unique size of Ca^{2+}. This size selection is supported by the inhibitory effects by several lanthanides (Gd^{3+}, Yb^{3+}, Lu^{3+}) that are Ca^{2+} surrogates of similar ionic radius. Based on the interkindom-mediated functional complementation of Ca^{2+} flux in mammalian cells by BsYetJ, it is feasible to assume that all TMBIM proteins possess Ca^{2+} flux activity. Furthermore, it seems likely that TMBIM family members share an ion recognition pattern that is similar to that of BsYetJ, but this hypothesis requires experimental validation through studies targeting eukaryotic family members. In our SPA measurements performed at different pHs, we found that Ca^{2+} binding follows a bell-shaped curve with a maximum at around pH 7.5 (Figure 3C). At this pH, BsYetJ wild-type is much more active than the two dyad mutants, suggesting that the sensor can effectively detect environmental changes in pH, undergo protonation steps, and conduct Ca^{2+} flux. These observations correlate very well with recent work showing that Ca^{2+} flux through the C-terminal peptide corresponding to TMBIM6's Ca^{2+}-channel- pore domain displays a bell-shaped dependence towards pH (Kiviluoto et al., 2013).

In bacteria, the physiological roles of TMBIM-mediated Ca^{2+} leak remain elusive. Nevertheless, intracellular Ca^{2+} is key to bacterial chemotaxis, mobility, virulence, and adaptation to environment (Dominguez et al., 2015). Although there are no intracellular Ca^{2+} stores in bacteria, several components of the Ca^{2+} signaling toolkits are expressed, including Ca^{2+}-binding proteins and Ca^{2+}- transport systems, such as P-type ATPases, electrochemical potential driven transporters and channels (Dominguez, 2004; Shemarova and Nesterov, 2014; Dominguez et al., 2015). While basal cytosolic [Ca^{2+}] in prokaryotes is kept low in the 100-300 nM range, cytosolic [Ca^{2+}] can transiently rise in responses to nitrogen starvation, environmental stress, and production of metabolites (Dominguez et al., 2015). Consequently, the expression of hundreds of genes is affected transiently by the increased cytosolic [Ca^{2+}], indicating a key role for Ca^{2+} signaling in the control of physiological processes in bacteria (Dominguez et al., 2015).

STAR*Methods

Contact for Reagent and Resource Sharing

Further information and reasonable requests for resources and reagents should be directed to and will be fulfilled by the Lead Contact, Qun Liu (qunliu@bnl.gov).

Experimental Model and Subject Details

Cell Culture—Adherent HeLa cells were cultured in DMEM medium (Invitrogen) at 37 °C and 5% CO_2. The culture was supplemented with 10% FBS (Invitrogen). For maintenance, HeLa cells were sub-cultured twice a week and at least three passages were performed prior to experiments.

Method Details

Protein Production—Expression and purification of N-terminal truncation (Δ5BsYetJ), ^{D195E}BsYetJ, and ^{D171E}BsYetJ were performed using the previously established protocols for the wild-type BsYetJ (Chang et al., 2014). Briefly, ^{D195E}BsYetJ and ^{D171E}BsYetJ mutations were generated by using a QuikChange Site-directed mutagenesis kit. pMCSG7 plasmid harboring the wild-type *YetJ* gene (Chang et al., 2014) was used as template to generate the two mutations. For the ^{D171E}BsYetJ mutation, primers 5'-ttttccctttacattttgtatgagttgaaccaaatcaagcaccgcca-3' (F) and 5'-tggcggtgcttgatttggttcaactcatacaaaatgtaaagggaaaa-3' (R) were used. For the ^{D195E}BsYetJ mutation, primers 5'-ggcgttatcgctgtacctagagtttatcaacttgttcatcaac-3' (F) and 5'-gttgatgaacaagttgataaactctaggtacagcgataacgcc-3' (R) were used. Both mutations were verified by sequencing. Protein expression was conducted in *Escherichia coli* BL21 pLysS cells growing in Terrific Broth medium. All purification steps were performed at 4 °C. Frozen cell pellets were suspended in a suspension buffer that contains 50 mM HEPES, pH 7.8, 300 mM NaCl, and 20 mM imidazole, 5% glycerol, and 1 mM $MgCl_2$. Cells were lysed by using an EmulsiFlex-C3 homogenizer (Avestin, Ottawa, Canada); and cell debris was removed by centrifugation at 15,000g for 30 min. Membranes were collected by centrifugation at 150,000g for 60 min and solubilized by addition of n-dodecyl β-D- maltopyranoside (DDM) to a final concentration of 1.5% (w/v) for 2 hrs. Cleaned-up supernatant was loaded to a HisTrap™ FF column (GE Healthcare, Inc.) and the protein was eluted by a linear gradient concentration of imidazole from 75 mM to 500 mM in the buffer of 50 mM HEPES, pH 7.8, 300 mM NaCl, 5% glycerol and 0.05% DDM. The affinity tag was cleaved by overnight incubation with sufficient amount of tobacco etch virus (TEV) protease and the enzyme was then removed by a second passage through the nickel column. The flow-through was concentrated and detergent was changed to n- dodecyl-N,N-dimethylamine-N-oxide (LDAO) by gel-filtration on a Superdex 200 10/300 GL column (GE Healthcare, Inc) with an elution buffer containing 25 mM Tris-HCl pH 8.0, 400 mM NaCl, 0.05% LDAO (w/v). Purified protein was concentrated to 10-13 mg/mL with an Amicon Ultra-15 centrifugal filter (Milipore, Inc).

Crystallization—For LCP crystallization, we used the N-terminal truncations (Δ5BsYetJ). To make lipidic cubic phase, we mixed 10 μL of protein (10 mg/mL) with 15 μL of monoolein (1:1.5 v/v) to get 40% hydration. Crystals were grown from the condition by mixing 50 nL of LCP with 800 nL of precipitant that contained 0.1 M Tris, pH 7.8, 5% PGA-LM (w/v), and 30% PEG 400 (v/v). The LCP crystals were harvested and cryocooled for cryogenic data collection.

For crystallization of ^{D171E}BsYetJ and ^{D195E}BsYetJ mutants, equal volumes of protein (10-12 mg/mL) in detergent LDAO were mixed with precipitants that contained 0.1 M

MOPS, pH 7.5, 38% PEG 400, and 0.2 M NaCl (for ^{D171E}BsYetJ) or 0.1 M ADA, pH 7.0, 30% PEG 600 (v/v) (for ^{D195E}BsYetJ). For both conditions, only needles crystals were obtained. These needles were harvested and cryocooled for cryogenic data collection.

Structure Determination—Diffraction data were collected at National Synchrotron Light source (NSLS) beamline X25 with a Quantum 315R detector and Advanced Photon Source (APS) NE-CAT 24-ID-C beamline with a Pilatus 6M detector under a cryogenic temperature of 100 K. All data sets were indexed and integrated by XDS (Kabsch, 2010) and scaled and merged by CCP4 program AIMLESS (Winn et al., 2011). Data collection and reduction statistics for single and multi-crystal data sets are listed in Table 1.

Structures were determined by molecular replacement method by PHASER (Read and McCoy, 2011) with starting model of either the closed or open state (Chang et al., 2014). Specifically, for the LCP structure, we used the closed state structure at pH 8 (PDB code 4PGR) for molecular replacement; and for the two mutants, we tried both the closed (PDB code 4PGR) and the open state structures (PDB code 4PGS). The LCP crystal was crystallized in space group $P2_1$ and molecular replacement solution is performed with only one molecule in asymmetric unit. The two mutants were both crystallized in space group C2 with four molecules in an asymmetric unit. Molecular replacement with the open-state structure gave the highest Z score as reported by PHASER.

The three structures were refined by CCP4 program REFMAC5 and PHENIX (Adams et al., 2010; Murshudov et al., 2011). Model and solvent adjustment and validation were performed iteratively with COOT (Brown et al., 2015) and PHENIX (Afonine et al., 2012). For the two mutant structures, non- crystallographic symmetry was used for restraints and TLS parameters were refined to model anisotropy. The stereochemistry of refined structures was validated with PROCHECK (Laskowski et al., 1993) and MOLPROBITY (Chen et al., 2010) for quality assurance. Data statistics for refinements were listed in Table 1.

Unidirectional $^{45}Ca^{2+}$-flux assay in HeLa cells—Unidirectional $^{45}Ca^{2+}$ efflux assays were performed following the previously established protocols (Luyten et al., 2014). We performed the experiments in 24-well tissue culture plates of which only 12 wells were analyzed. Confluent monolayers of HeLa cells were obtained by seeding 30,000 cells per well and growing them for 7 days at 37 °C and 5% CO_2 in DMEM medium. The culture medium was removed, and the cells were permeabilized in a solution containing 120 mM KCl, 30 mM imidazole-HCl, pH 6.8, 2 mM $MgCl_2$, 1 mM Na-ATP, 1 mM K-EGTA, and 20 μg saponin ml^{-1}. After permeabilization for 10 mins at 25 °C, Ca^{2+} stores were loaded for 45 min with $^{45}Ca^{2+}$ in a solution containing 120 mM KCl, 30 mM imidazole-HCl, pH 6.8, 5 mM MgCh, 5 mM Na-ATP, 0.44 mM K-EGTA, and 150 nM free Ca^{2+} mixed with $^{45}Ca^{2+}$ (with a specific activity of 0.3 MBq/mL). Then, 200 μl of efflux buffer containing 120 mM KCl, 30 mM imidazole-HCl, pH 6.8, and 1 mM K-EGTA was added and removed every 2 min. The indicated BsYetJ (2.5 mM) or buffer was added. At the end of each experiment, the $^{45}Ca^{2+}$ remnant in the ER was determined by incubating with 200 μl of 2% (w/v) SDS solution for 30 min.

Scintillation Proximity Assay (SPA)—Binding of $^{45}Ca^{2+}$ by BsYetJ wild-type and its mutants was measured with the SPA. For the assay 50 ng of protein was incubated with 10 μM $^{45}Ca^{2+}$ (746 Ci/mmol) in the presence of 2.5 mg/mL YSi His tag SPA beads in 500 mM Tris/MES, with a pH ranging from pH 6.0 to 8.0, 20% glycerol (w/v), 0.1 % DDM (w/v) and 1 mM TCEP. Tris/MES was equimolarly replaced with indicated salts. The specific cpm of $^{45}Ca^{2+}$ binding was determined by subtracting the non-proximity-based cpm, determined in the presence of 400 mM imidazole which prevents binding of the His-tagged recombinant protein to the YSi His tag SPA beads, from the total signal). Data of representative figures are shown as the mean ± S.E.M of triplicate determinations with at least three independent repeats. Non-linear regression fitting was performed in Sigma Plot 13 (Systat software), and the results are shown as mean ± S.E.M. of the fit.

Molecular Dynamics Simulations—The molecular models were all constructed starting from the closed-state structure of the wild-type YetJ (PDB ID 4PGR). MD simulations of these models were performed in the explicit water and 1-palmitoyl- 2-oleoylphosphatidylcholine (POPC) lipid bilayer environment using Desmond MD System (version 4.5; D. E. Shaw Research, New York, NY) with the CHARMM36 force field (MacKerell et al., 1998; MacKerell et al., 2004; Klauda et al., 2010; Best et al., 2012) and TIP3P water model. The system charges were neutralized, and 150 mM NaCl was added. The average size of the simulation systems was ~68000 atoms. The Protein-membrane relaxation was carried out with a protocol modified from that developed by Schrodinger, LLC. Briefly, the initial energy minimization was followed by equilibration with restraints on all protein and ligand heavy atoms in the beginning for 1 ns, then with restraints only on the protein backbone for 6 ns. For both the equilibrations and the following unrestrained production runs, we used Langevin constant pressure and temperature dynamical system (Feller et al., 1995) to maintain the pressure at 1 atm and the temperature at 310K, on an anisotropic flexible periodic cell with a constant-ratio constraint applied on the lipid bilayer in the X-Y plane.

For each condition, we collected multiple trajectories: WT Asp171-deprotonated (2 trajectories, totally 3.6 μs), WT Asp171-protonated (8 trajectories, totally 10.8 pμs), D171E Glu171-deprotonated (10 trajectories, totally 6 μs), D171E Glu171-protonated (10 trajectories, totally 6 μs). Figure 4 consists the representative frames of each condition.

Quantification and Statistical Analysis

Unidirectional flux experiments were done in duplicates with purified protein sample. SPA experiments were done in triplicates with purified protein samples.

Data and Software Availability

Data Resources—Atomic coordinates and structure factor files have been deposited in the RCSB Protein Data Bank (PDB) under the accession code 6NQ7 for wild-type ^{LCP}BsYetJ structure, 6NQ8 for ^{D171E}BsYetJ structure, and 6NQ9 for ^{D195E}BsYetJ structure.

Supplementary Material

Refer to Web version on PubMed Central for supplementary material.

Acknowledgements

This project was supported by BNL LDRD 17-023 to Q.L., NIDA IRP Z1A DA000606-03 to L.S., and NIH R01 GM119396 to M.Q. Work in the lab of G.B. was supported by grants from the Research Council – KU Leuven (OT/14/101) and Research Foundation – Flanders (FWO grants G.0901.18 and W0.019.17N). We thank beamline staff at NSLS X25, NSLS-II FMX and AMX, and APS NE-CAT for their assistance in crystal screening and data collection. Part of this work was conducted at NE-CAT which is funded by NIH P30 GM124165 and S10 RR029205. This research used resources of the National Synchrotron Light source II and Advanced Photon Source, two U.S. Department of Energy Office of Science User Facilities operated under Contract No. DE-SC0012704 and DE-AC02-06CH11357, respectively.

References

Adams PD, Afonine PV, Bunkoczi G, Chen VB, Davis IW, Echols N, Headd JJ, Hung LW, Kapral GJ, Grosse-Kunstleve RW, et al. (2010). PHENIX: a comprehensive Python-based system for macromolecular structure solution. Acta Crystallogr D 66, 213–221. [PubMed: 20124702]

Afonine PV, Grosse-Kunstleve RW, Echols N, Headd JJ, Moriarty NW, Mustyakimov M, Terwilliger TC, Urzhumtsev A, Zwart PH, and Adams PD (2012). Towards automated crystallographic structure refinement with phenix.refine. Acta Crystallogr D 68, 352–367. [PubMed: 22505256]

Ahn T, Yun CH, Chae HZ, Kim HR, and Chae HJ (2009). Ca^{2+}/H^{+} antiporter-like activity of human recombinant Bax inhibitor-1 reconstituted into liposomes. FEBS J 276, 2285–2291. [PubMed: 19290886]

Berridge MJ, Bootman MD, and Roderick HL (2003). Calcium signalling: dynamics, homeostasis and remodelling. Nat Rev Mol Cell Biol 4, 517–529. [PubMed: 12838335]

Best RB, Zhu X, Shim J, Lopes PEM, Mittal J, Feig M, and MacKerell AD (2012). Optimization of the Additive CHARMM All-Atom Protein Force Field Targeting Improved Sampling of the Backbone phi, psi and Side-Chain chi(1) and chi(2) Dihedral Angles. J Chem Theory Comput 8, 3257–3273. [PubMed: 23341755]

Bittremieux M, Parys JB, Pinton P, and Bultynck G (2016). ER functions of oncogenes and tumor suppressors: Modulators of intracellular Ca^{2+} signaling. Mol Cell Res 1863, 1364–1378.

Brown A, Long F, Nicholls RA, Toots J, Emsley P, and Murshudov G (2015). Tools for macromolecular model building and refinement into electron cryo-microscopy reconstructions. Acta Crystallogr D 71, 136–153. [PubMed: 25615868]

Bultynck G, Kiviluoto S, Henke N, Ivanova H, Schneider L, Rybalchenko V, Luyten T, Nuyts K, De Borggraeve W, and Bezprozvanny I (2012). The C terminus of Bax inhibitor-1 forms a Ca^{2+}-permeable channel pore. J Biol Chem 287, 2544–2557. [PubMed: 22128171]

Bultynck G, Kiviluoto S, and Methner A (2014). Bax inhibitor-1 is likely a pH-sensitive calcium leak channel, not a $H^{+}/Ca2^{+}$ exchanger. Sci Signal 7, pe22–pe22. [PubMed: 25227609]

Carafoli E, and Krebs J (2016). Why Calcium? How Calcium Became the Best Communicator. J Biol Chem 291, 20849–20857. [PubMed: 27462077]

Carrara G, Parsons M, Saraiva N, and Smith GL (2017). Golgi anti-apoptotic protein: a tale of camels, calcium, channels and cancer. Open Biol 7.

Carrara G, Saraiva N, Parsons M, Byrne B, Prole DL, Taylor CW, and Smith GL (2015). Golgi anti-apoptotic proteins are highly conserved ion channels that affect apoptosis and cell migration. J Biol Chem 290, 11785–11801. [PubMed: 25713081]

Chae HJ, Kim HR, Xu CY, Bailly-Maitre B, Krajewska M, Krajewski S, Banares S, Cui J, Digicaylioglu M, Ke N, et al. (2004). BI-1 regulates an apoptosis pathway linked to endoplasmic reticulum stress. Mol Cell 15, 355–366. [PubMed: 15304216]

Chang Y, Bruni R, Kloss B, Assur Z, Kloppmann E, Rost B, Hendrickson WA, and Liu Q (2014). Structural basis for a pH-sensitive calcium leak across membranes. Science 344, 1131–1135. [PubMed: 24904158]

Chen VB, Arendall WB, Headd JJ, Keedy DA, Immormino RM, Kapral GJ, Murray LW, Richardson JS, and Richardson DC (2010). MolProbity: all-atom structure validation for macromolecular crystallography. Acta Crystallogr D 66, 12–21. [PubMed: 20057044]

de Mattia F, Gubser C, van Dommelen MM, Visch HJ, Distelmaier F, Postigo A, Luyten T, Parys JB, de Smedt H, Smith GL, et al. (2009). Human Golgi antiapoptotic protein modulates intracellular calcium fluxes. Mol Biol Cell 20, 3638–3645. [PubMed: 19553469]

Dominguez DC (2004). Calcium signalling in bacteria. Mol Microbiol 54, 291–297. [PubMed: 15469503]

Dominguez DC, Guragain M, and Patrauchan M (2015). Calcium binding proteins and calcium signaling in prokaryotes. Cell Calcium 57, 151–165. [PubMed: 25555683]

Feller SE, Zhang YH, Pastor RW, and Brooks BR (1995). Constant-pressure molecular- dynamics simulation - the Langevin piston method. J Chem Phys l03, 4613–4621.

Gamboa-Tuz SD, Pereira-Santana A, Zhao T, Schranz ME, Castano E, and Rodriguez-Zapata LC (2018). New Insights into the Phylogeny of the TMBIM Superfamily across the Three of Life: Comparative Genomics and Synteny Networks Reveal Independent Evolution of the BI and LFG Families in Plants. Mol Phylogenet Evol 126, 266–278. [PubMed: 29702215]

Grzmil M, Kaulfuss S, Thelen P, Hemmerlein B, Schweyer S, Obenauer S, Kang TW, and Burfeind P (2006). Expression and functional analysis of Bax inhibitor-1 in human breast cancer cells. J Pathol 208, 340–349. [PubMed: 16353131]

Henke N, Lisak DA, Schneider L, Habicht J, Pergande M, and Methner A (2011). The ancient cell death suppressor BAX inhibitor-1. Cell Calcium 50, 251–260. [PubMed: 21663964]

Hu L, Smith TF, and Goldberger G (2009). LFG: a candidate apoptosis regulatory gene family. Apoptosis 14, 1255–1265. [PubMed: 19784873]

Ishikawa T, Watanabe N, Nagano M, Kawai-Yamada M, and Lam E (2011). Bax inhibitor-1: a highly conserved endoplasmic reticulum-resident cell death suppressor. Cell Death Differ 18, 1271–1278. [PubMed: 21597463]

Kabsch W (2010). XDS. Acta Crystallogr D 66, 125–132. [PubMed: 20124692]

Kim HR, Lee GH, Ha KC, Ahn T, Moon JY, Lee BJ, Cho SG, Kim S, Seo YR, and Shin YJ (2008). Bax Inhibitor-1 Is a pH-dependent regulator of Ca^{2+} channel activity in the endoplasmic reticulum. J Biol Chem 283, 15946–15955. [PubMed: 18378668]

Kiviluoto S, Luyten T, Schneider L, Lisak D, Rojas-Rivera D, Welkenhuyzen K, Missaen L, De Smedt H, Parys JB, and Hetz C (2013). Bax inhibitor-1-mediated Ca^{2+} leak is decreased by cytosolic acidosis. Cell Calcium 54, 186–192. [PubMed: 23867001]

Klauda JB, Venable RM, Freites JA, O'Connor JW, Tobias DJ, Mondragon-Ramirez C, Vorobyov I, MacKerell AD, and Pastor RW (2010). Update of the CHARMM all-atom additive force field for lipids: validation on six lipid types. J Phys Chem B 114, 7830–7843. [PubMed: 20496934]

Krajewska M, Xu L, Xu WJ, Krajewski S, Kress CL, Cui JK, Yang L, Irie F, Yamaguchi Y, Lipton SA, et al. (2011). Endoplasmic reticulum protein BI-1 modulates unfolded protein response signaling and protects against stroke and traumatic brain injury. Brain Research 1370, 227–237. [PubMed: 21075086]

Laskowski RA, Macarthur MW, Moss DS, and Thornton JM (1993). Procheck - a program to check the stereochemical quality of protein structures. J Appl Crystallogr 26, 283–291.

Leanza L, Biasutto L, Manago A, Gulbins E, Zoratti M, and Szabo I (2013). Intracellular ion channels and cancer. Front Physiol 4, 227. [PubMed: 24027528]

Lee G-H, Ahn T, Kim D-S, Park SJ, Lee YC, Yoo WH, Jung SJ, Yang J-S, Kim S, and Muhlrad A (2010). Bax inhibitor 1 increases cell adhesion through actin polymerization: involvement of calcium and actin binding. Mol Cell Biol 30, 1800–1813. [PubMed: 20123969]

Lisak D, Schacht T, Gawlitza A, Albrecht P, Aktas O, Koop B, Gliem M, Hofstetter HH, Zanger K, Bultynck G, et al. (2016). BAX inhibitor-1 is a Ca^{2+} channel critically important for immune cell function and survival. Cell Death Differ 23, 358–368. [PubMed: 26470731]

Lisak DA, Schacht T, Enders V, Habicht J, Kiviluoto S, Schneider J, Henke N, Bultynck G, and Methner A (2015). The transmembrane Bax inhibitor motif (TMBIM) containing protein family: Tissue expression, intracellular localization and effects on the ER CA2+-filling state. Mol Cell Res 1853, 2104–2114.

Liu Q (2017). TMBIM-mediated Ca^{2+} homeostasis and cell death. Mol Cell Res 1864, 850–857.

Lu B, Li Y, Li H, Zhang Y, Xu J, Ren L, Fu S, and Zhou Y (2015). Bax inhibitor-1 is overexpressed in non-small cell lung cancer and promotes its progression and metastasis. Int J Clin Exp Pathol 8, 1411–1418. [PubMed: 25973025]

Luganini A, Di Nardo G, Munaron L, Gilardi G, Pla AF, and Gribaudo G (2018). Human cytomegalovirus US21 protein is a viroporin that modulates calcium homeostasis and protects cells against apoptosis. Proc Natl Acad Sci USA 115, E12370–E12377. [PubMed: 30530673]

Luyten T, Bultynck G, Parys JB, De Smedt H, and Missiaen L (2014). Measurement of intracellular Ca^{2+} release in permeabilized cells using $45Ca^{2+}$. CSH Protoc 2014, pdb. prot073189.

MacKerell AD, Bashford D, Bellott M, Dunbrack RL, Evanseck JD, Field MJ, Fischer S, Gao J, Guo H, Ha S, et al. (1998). All-atom empirical potential for molecular modeling and dynamics studies of proteins. J Phys Chem B 102, 3586–3616. [PubMed: 24889800]

MacKerell AD, Feig M, and Brooks CL (2004). Improved treatment of the protein backbone in empirical force fields. J Amer Chem Soc 126, 698–699. [PubMed: 14733527]

Mattson MP, and Chan SL (2003). Calcium orchestrates apoptosis. Nat Cell Biol 5, 1041–1043. [PubMed: 14647298]

Merianda TT, Vuppalanchi D, Yoo S, Blesch A, and Twiss JL (2013). Axonal transport of neural membrane protein 35 mRNA increases axon growth. J Cell Sci 126, 90–102. [PubMed: 23097042]

Murshudov GN, Skubak P, Lebedev AA, Pannu NS, Steiner RA, Nicholls RA, Winn MD, Long F, and Vagin AA (2011). REFMAC5 for the refinement of macromolecular crystal structures. Acta Crystallogr D 67, 355–367. [PubMed: 21460454]

Oka T, Sayano T, Tamai S, Yokota S, Kato H, Fujii G, and Mihara K (2008). Identification of a novel protein MICS1 that is involved in maintenance of mitochondrial morphology and apoptotic release of cytochrome c. Mol Biol Cell 19, 2597–2608. [PubMed: 18417609]

Pinton P, Giorgi C, Siviero R, Zecchini E, and Rizzuto R (2008). Calcium and apoptosis: ER-mitochondria Ca2+ transfer in the control of apoptosis. Oncogene 27, 6407–6418. [PubMed: 18955969]

Quick M, and Javitch JA (2007). Monitoring the function of membrane transport proteins in detergent-solubilized form. Proc Natl Acad Sci USA 104, 3603–3608. [PubMed: 17360689]

Read RJ, and McCoy AJ (2011). Using SAD data in Phaser. Acta Crystallogr D 67, 338–344. [PubMed: 21460452]

Reich A, Spering C, Gertz K, Harms C, Gerhardt E, Kronenberg G, Nave KA, Schwab M, Tauber SC, Drinkut A, et al. (2011). Fas/CD95 regulatory protein Faim2 is neuroprotective after transient brain ischemia. J Neurosci 31, 225–233. [PubMed: 21209208]

Reimers K, Choi CYU, Bucan V, and Vogt PM (2008). The Bax Inhibitor-1 (BI-1) family in apoptosis and tumorigenesis. Curr Mol Med 8, 148–156. [PubMed: 18336295]

Rojas-Rivera D, Armisen R, Colombo A, Martinez G, Eguiguren AL, Diaz A, Kiviluoto S, Rodriguez D, Patron M, Rizzuto R, et al. (2012). TMBIM3/GRINA is a novel unfolded protein response (UPR) target gene that controls apoptosis through the modulation of ER calcium homeostasis. Cell Death Differ 19, 1013–1026. [PubMed: 22240901]

Rojas-Rivera D, and Hetz C (2015). TMBIM protein family: ancestral regulators of cell death. Oncogene 34, 269–280. [PubMed: 24561528]

Sano R, Hou YCC, Hedvat M, Correa RG, Shu CW, Krajewska M, Diaz PW, Tamble CM, Quarato G, Gottlieb RA, et al. (2012). Endoplasmic reticulum protein BI-1 regulates Ca^{2+}- mediated bioenergetics to promote autophagy. Gene Dev 26, 1041–1054. [PubMed: 22588718]

Saraiva N, Prole DL, Carrara G, Johnson BF, Taylor CW, Parsons M, and Smith GL (2013). hGAAP promotes cell adhesion and migration via the stimulation of store-operated Ca^{2+} entry and calpain 2. J Cell Biol 202, 699–713. [PubMed: 23940116]

Shemarova IV, and Nesterov VP (2014). Ca^{2+} signaling in prokaryotes. Microbiology 83, 431–437.

Shukla S, Fujita K, Xiao Q, Liao Z, Garfield S, and Srinivasula SM (2011). A shear stress responsive gene product PP1201 protects against Fas-mediated apoptosis by reducing Fas expression on the cell surface. Apoptosis 16, 162–173. [PubMed: 21107705]

Sokolov S, Scheuer T, and Catterall WA (2007). Gating pore current in an inherited ion channelopathy. Nature 446, 76. [PubMed: 17330043]

Urresti J, Ruiz-Meana M, Coccia E, Arevalo JC, Castellano J, Fernandez-Sanz C, Galenkamp KMO, Planells-Ferrer L, Moubarak RS, Llecha-Cano N, et al. (2016). Lifeguard inhibits Fas ligand-mediated endoplasmic reticulum-calcium release mandatory for apoptosis in Type II apoptotic cells. J Biol Chem 291, 1221–1234. [PubMed: 26582200]

Winn MD, Ballard CC, Cowtan KD, Dodson EJ, Emsley P, Evans PR, Keegan RM, Krissinel EB, Leslie AG, and McCoy A (2011). Overview of the CCP4 suite and current developments. Acta Crystallogr D 67, 235–242. [PubMed: 21460441]

Xu C, Xu W, Palmer AE, and Reed JC (2008). BI-1 regulates endoplasmic reticulum Ca^{2+} homeostasis downstream of Bcl-2 family proteins. J Biol Chem 283, 11477–11484. [PubMed: 18299329]

Xu Q, and Reed JC (1998). Bax inhibitor-1, a mammalian apoptosis suppressor identified by functional screening in yeast. Mol Cell 1, 337–346. [PubMed: 9660918]

Yoshisue H, Suzuki K, Kawabata A, Ohya T, Zhao H, Sakurada K, Taba Y, Sasaguri T, Sakai N, and Yamashita S (2002). Large scale isolation of non-uniform shear stress-responsive genes from cultured human endothelial cells through the preparation of a subtracted cDNA library. Atherosclerosis 162, 323–334. [PubMed: 11996952]

Zehnpfennig B, Wiriyasermkul P, Carlson DA, and Quick M (2015). Interaction of alpha-lipoic acid with the human Na^{+}/multivitamin transporter (hSMVT). J Biol Chem 290, 16372–16382. [PubMed: 25971966]

Highlights:

- BsYetJ mediates Ca^{2+} flux in mammalian cells
- The Ca^{2+}-binding activity is sensitive to protons and other cations
- The Asp171-Asp195 dyad controls pore opening and pH-dependent Ca^{2+} binding
- Protonation of Asp171 leads to an open-state structure

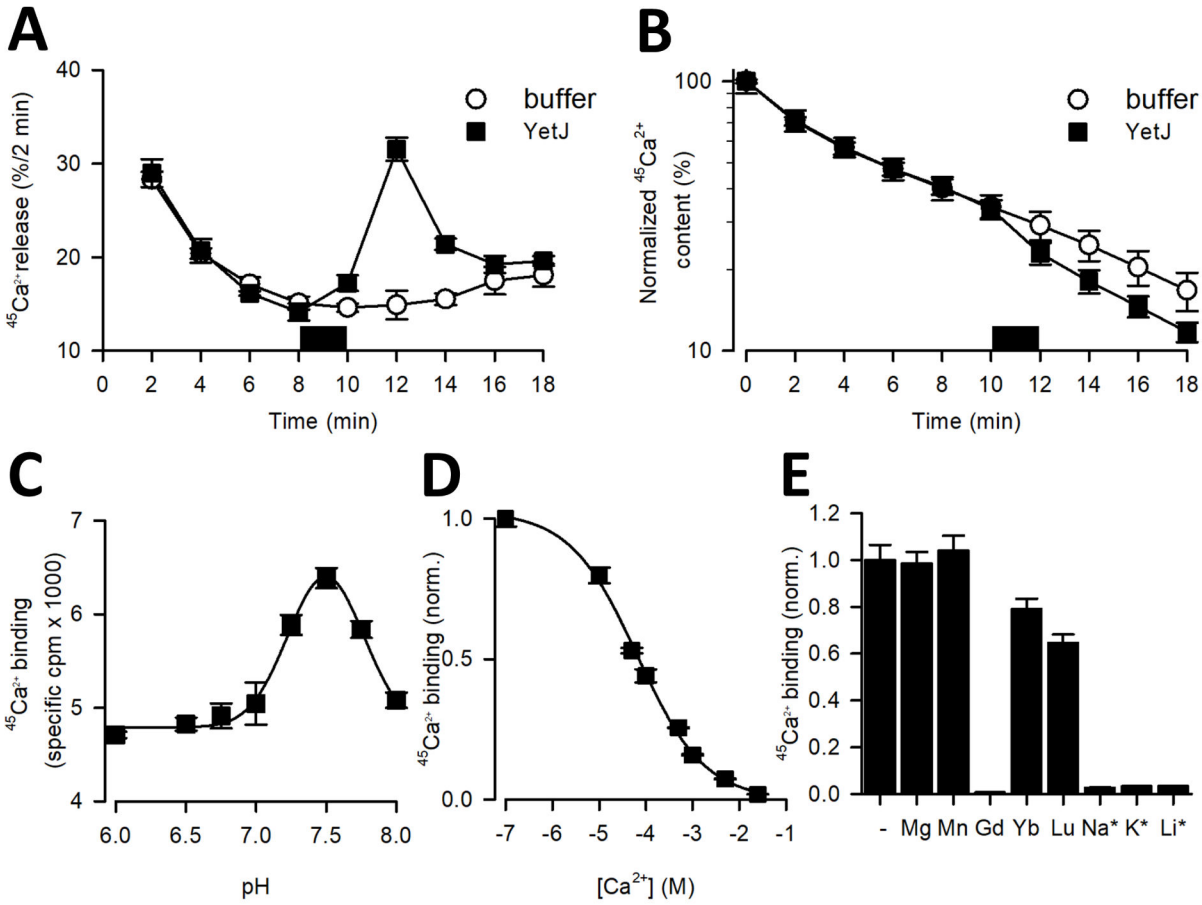

Figure 1. Ca^{2+} activity of BsYetJ.

(**A-B**) Ca^{2+} efflux mediated by BsYetJ. Permeabilized HeLa cells loaded to steady-state with $^{45}Ca^{2+}$ were incubated in Ca^{2+}-free efflux medium. $^{45}Ca^{2+}$ release (% / 2 min) was plotted as a function of time (**A**) and normalized $^{45}Ca^{2+}$ content (%) was plotted as a function of time (**B**). In the time period indicated by the dark square, buffer or BsYetJ (2.5 mM) was added for 2 min. Data from a typical experiment are represented as mean ± SD (n= 2; i.e. duplicate technical repeats). The graph is representative for 3 independent experiments. (**C**) pH dependence of $^{45}Ca^{2+}$ binding. Binding of 10 μM $^{45}Ca^{2+}$ (746 Ci/mmol) to 50 ng of BsYetJ was measured in assay buffer with a pH ranging from 6.0 to 8.0. Data were fit to a Gaussian model, revealing a peak at pH 7.46 ± 0.01. (**D**) Apparent affinity of Ca^{2+} binding by BsYetJ at pH 7.5. 10 μM $^{45}Ca^{2+}$ binding was measured in the presence of increasing concentrations of non-labeled Ca^{2+}, yielding an EC_{50} of 65.4 ± 0.9 μM. (**E**) Ion sensitivity of BsYetJ. 10 μM $^{45}Ca^{2+}$ binding by BsYetJ was measured in the absence (−) or presence of 5 mM or 100 mM (*) of the indicated cations. Data are represented as mean ± SEM (n= 3).

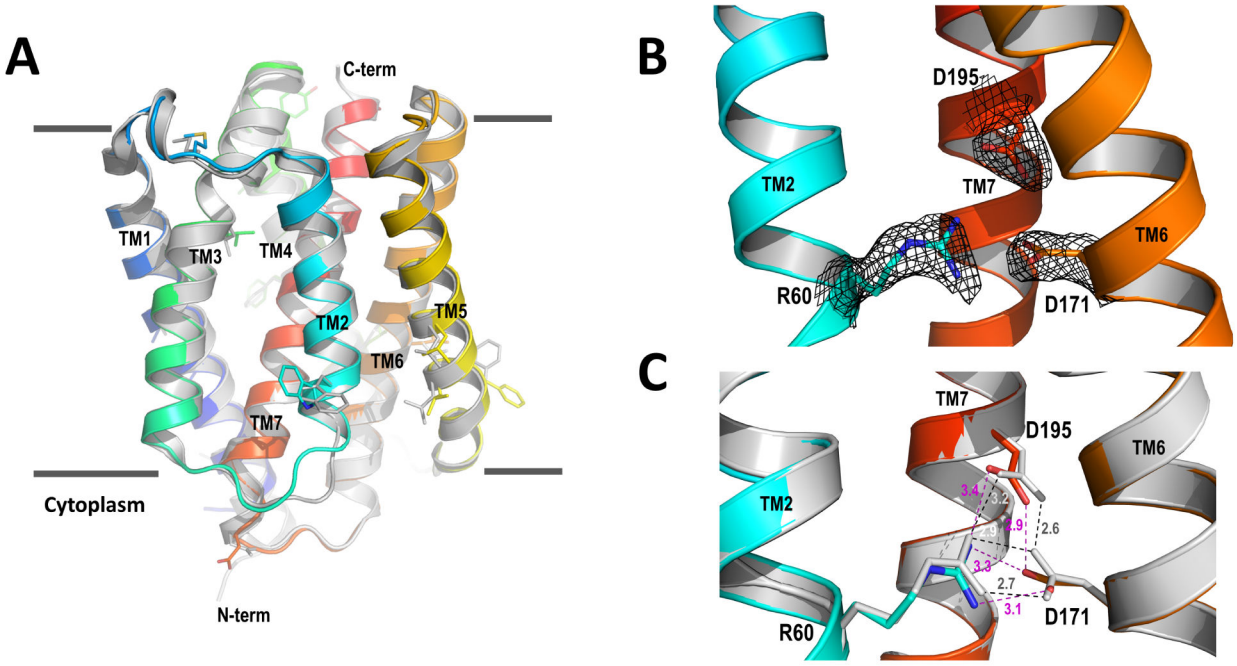

Figure 2. Crystal structure of BsYetJ in LCP.

(**A**) ^{LCP}BsYetJ structure superimposed with the structure crystallized from detergent C10E5 (^{C10E5}BsYetJ). (**B**) Electron densities for the aspartyl dyad pH sensor and the conformation latch Arg60. (**C**) Superimposition of ^{LCP}BsYetJ with ^{C10E5}BsYetJ for the aspartyl dyad and Arg60. Dash lines show distances between indicated residues, magenta for ^{LCP}BsYetJ and dark for ^{C10E5}BsYetJ.

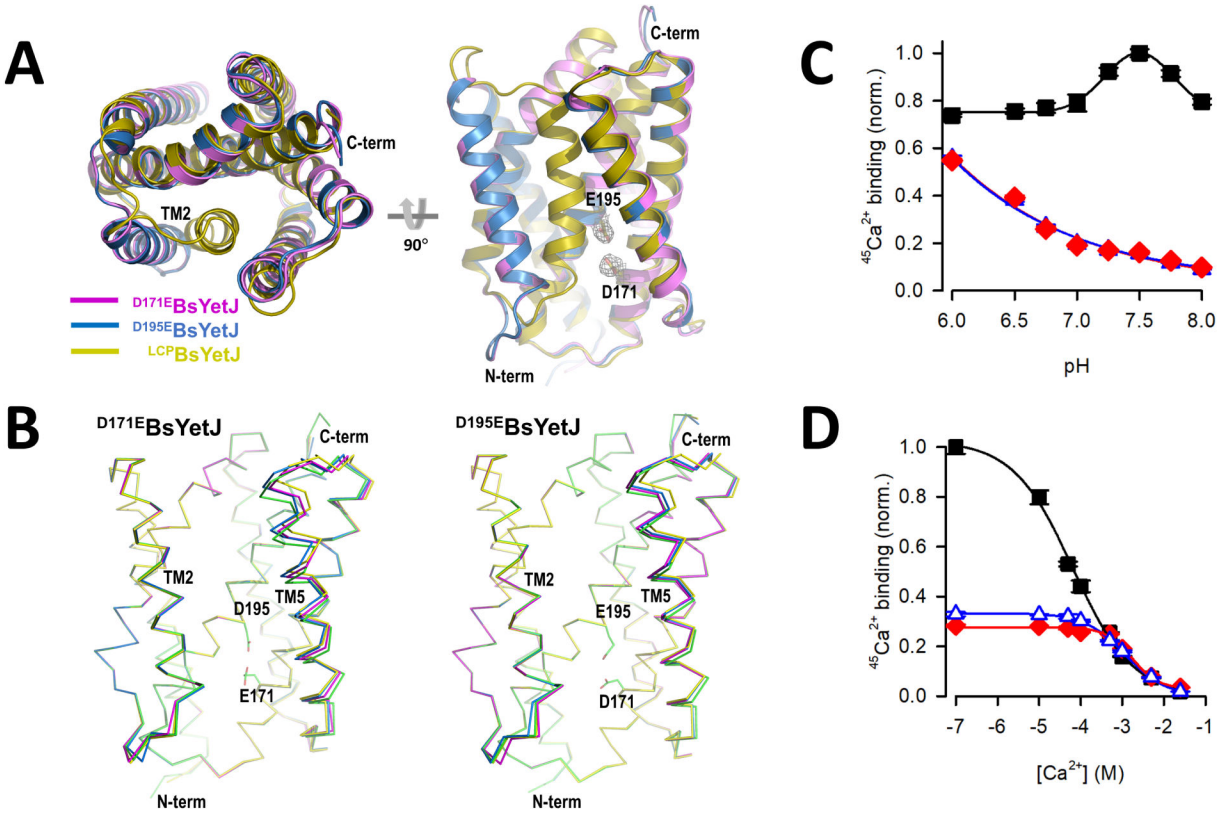

Figure 3. Structure and activity of two pH-sensitive mutants.

(**A**) Two views of structures of ^{D171E}BsYetJ and ^{D195E}BsYetJ. The two mutant structures were superimposed with ^{LCP}BsYetJ. Both mutant structures are open with TM2 unlocked from residue 171. (**B**) Superimpositions of the four molecules in crystallographic asymmetric unit indicate the flexibility of TM5 in ^{D171E}BsYetJ (**left**) and ^{D195E}BsYetJ (**right**). (**C**) pH-dependent Ca^{2+} binding by wild-type BsYetJ (■), ^{D171E}BsYetJ (♦), or ^{D195E}BsYetJ (Δ). (**D**) The EC_{50} of Ca^{2+} binding by wild-type (■), ^{D171E}BsYetJ (♦) or ^{D195E}BsYetJ (Δ) was determined by isotopic dilution of 10 μM $^{45}Ca^{2+}$ with non-radiolabeled $CaCl_2$, yielding apparent affinity constants of 64.2 ± 1.3 μM, 1.2 ± 0.1 mM, and 1.7 ± 0.3 mM, respectively. Data are represented as mean ± SEM (n=3).

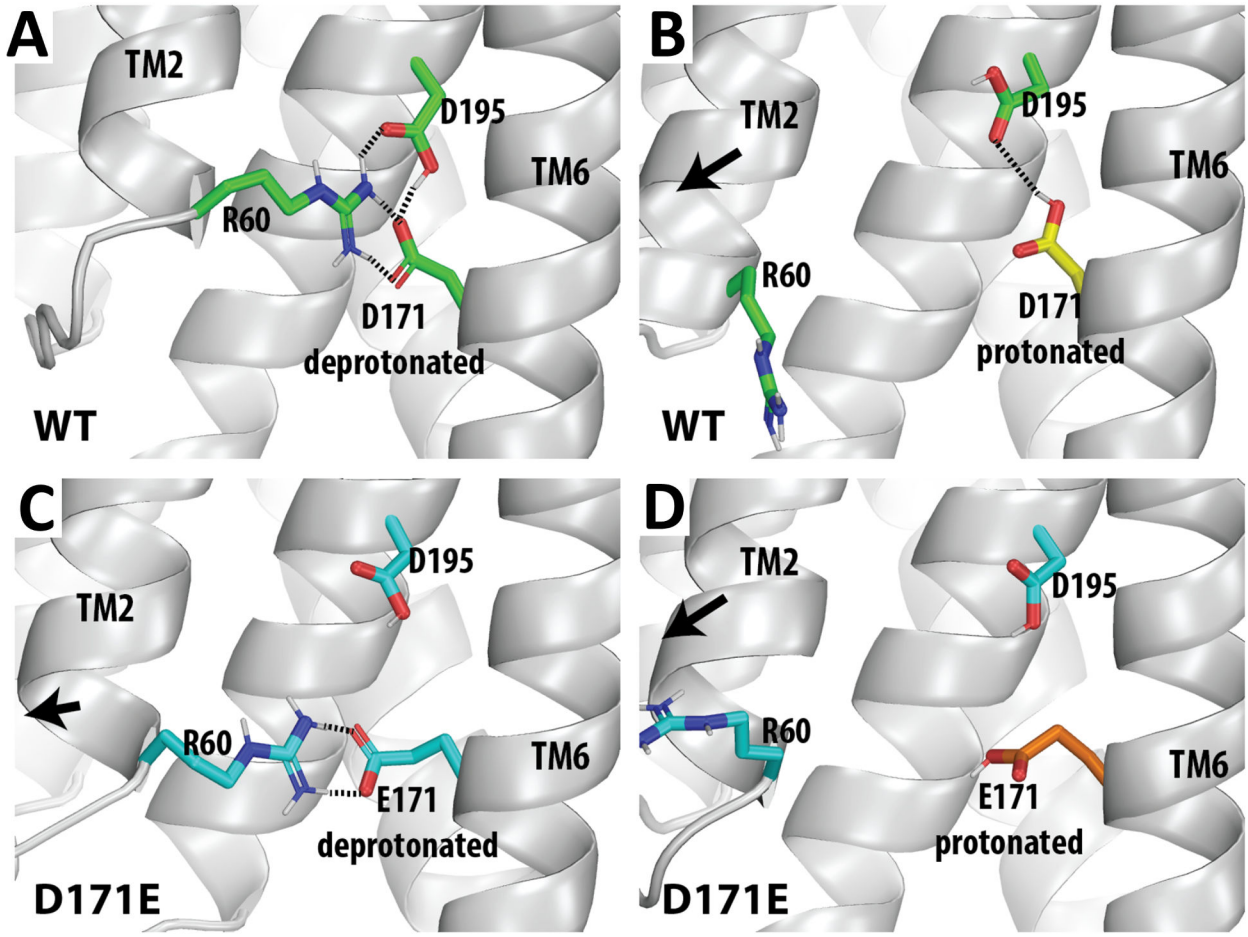

Figure 4. Molecular dynamics simulations of the Asp171-Asp195 dyad.

The results of MD simulations show that the mutation D171E and/or the protonation of the residue at this position disrupt the tight interactions among Arg60, Asp171, and Asp195, and result in a rearrangement of TM2 away from TM6. Representative frames of the simulations are shown for WT Asp171-deprotonated (**A**), WT Asp171-protonated (**B**), D171E Glu171-deprotonated (**C**), D171E Glu171-protonated (**D**). Note the Asp195 is protonated in all conditions. The interactions that are within the H-bond distance are indicated by dotted lines.

Table 1.

Data collection and refinement statistics

Data collection	**^{LCP}BsYetJ**	**^{D171E}BsYetJ**	**^{D195E}BsYetJ**
Wavelength (Å)	0.979	0.979	1.1
Space group	$P2_1$	C2	C2
Cell dimensions	33.86, 62.04, 47.34	218.09, 117.30, 52.41	217.33, 118.20, 51.89
a, b, c (Å) β (°)	93.95	92.96	93.23
Solvent content (%)	44.0	65.0	65.1
Bragg spacings (Å)	37.39-2.50 (2.63-2.50)	47.15-3.10 (3.31-3.10)	39.96-3.1 (3.31-3.10)
Total reflections	46387	76248	92561
Unique reflections	6634	23721	23817
Completeness (%)	95.3 (78.4)	99.1 (99.7)	99.8 (99.9)
I/σ(I)	6.0 (2.4)	5.4 (1.1)	6.0 (1.1)
$_{R}$meas	0.218 (0.939)	0.266 (1.429)	0.312 (2.124)
Multiplicity	7.0 (6.5)	3.2 (3.2)	3.9 (3.9)
$CC_{1/2}$	97.3 (77.0)	98.1 (36.6)	98.6 (37.2)
Refinement			
Resolution (Å)	2.5	3.1	3.1
No. reflections	6273	23641	23799
R_{work}/R_{free}	0.243/0.260	0.243/0.271	0.247/0.276
No. atoms	1624	6430	6416
Protein	1592	6430	6416
Water	31	-	-
Average B ($Å^2$)	39.6	61.53	68.0
Protein	39.5	61.53	68.0
Water	44.0	-	-
R.m.s deviations			
Bond length (Å)	0.007	0.002	0.002
Bond angle (°)	0.986	0.454	0.409
PDB code	6NQ7	6NQ8	6NQ9